Scientific Visualization, 2026, volume 18, number 3, pages 29 - 40, DOI: 10.26583/sv.18.3.03

Visualizing Attractor Basin Structures via the Method of Inverse Discrete-Dissipative Projections: A Case Study of the Lorenz System

G. Chernykh[1,A], A. Zhukova[2,B]

[A] Independent Researcher, Saint Petersburg, Russia
[B] Saint Petersburg Electrotechnical University "LETI", 5 Professora Popova St., 197376

[1] ORCID: 0000-0002-8093-3964, german.ch@chgerman.com
[2] ORCID: 0000-0003-0653-0427, millionnaya13@yandex.ru

Abstract

This article advances a numerical method for visualizing the structure of attractor basins in dynamical systems defined by ordinary differential equations. Herein, "structure" denotes any manner of inhomogeneity within the phase space, construed through the lens of a priori defined measurable characteristics. The method's foundation lies in discretizing the original mathematical model and monitoring the concomitant reduction of discrete phase volumes as the attractor is approached. The procedure starts from an initial condition, which is subsequently ascribed a numerical signature encapsulating the rate at which the phase volume that starts from that initial condition shrinks. These conditions are selected on a two-dimensional surface that forms a bounded region of a cross-section of the phase space. The visualization is generated by mapping the derived numerical signatures onto a prescribed color palette and projecting them onto the chosen domain. Experimental validation, conducted using the Lorenz system for both regular dynamics and parameters inducing a strange attractor, demonstrates the method's efficacy, particularly in revealing subtle structures that emerge in systems subjected to discretization.

Keywords: strange attractor, discretization, dissipation, attractor basin structure, inverse discrete-dissipative projections.

1. Introduction

The visualization method presented herein was conceived within the context of investigating nonlinear systems exhibiting deterministic chaotic dynamics [1-3]. Two fundamentally divergent approaches to studying chaotic systems exist; in a sense, both are philosophical constructs. The first, conventional approach employs the methods of classical continuum mathematics. The second is predicated upon A.N. Kolmogorov's theory of algorithmic information, known as Kolmogorov complexity [4], which is grounded in the concept of finite precision. The conceptual framework of Kolmogorov complexity constitutes the conceptual underpinning and primary motivation for our research. Within Kolmogorov's framework, as applied to chaotic systems, the classical conception of a trajectory is absent. Instead of trajectories — deemed uncomputable by Kolmogorov — one must consider either solutions obtained through regularization/discretization or functionals thereof. The computational method (algorithm), serving as the sole instrument for "observing" trajectories, becomes an integral component of the system itself. An analogy with quantum mechanics is apt: the equations governing the system's evolution assume the role of quantum objects, the act of observation consists in introducing regularization — practically manifested in the application of a specific numerical method — and the computational outcomes become the observables.

The implementation of any numerical method on a computational device inherently entails the discretization of the mathematical object under study. It is obvious that should the computation of a phase trajectory on a strange attractor be prolonged sufficiently, the trajectory will eventually close upon itself, a consequence of the finite precision and determinism of the computing machinery. Thus, the "observed" strange attractors "materialize" as sets of cycles. In [1, 2], systematic investigations into the discrete analogues of strange attractors, wherein the discretization scheme was specifically tailored to reflect the fundamental properties of algorithmic computation were undertaken. We herein recapitulate several pivotal findings.

The precision of discretization, formally expressed by the lattice step size in the system's phase space, dictates the ultimate complexity of the cycles comprising the discrete attractor. As the lattice step is refined, the complexity of these cycles increases predictably, while the average number of cycles remains largely conserved. The deliberate use of the term "ultimate complexity" is warranted, as minor perturbations of the lattice step around any given value yield not only discrete attractors of the maximum permissible complexity but also variants of any lesser complexity. A veritable "spectrum" of cycles emerges, representatives of which can be obtained with a certain probability by varying the discretization parameter. It is a curious fact that even under fine discretization — where the cycle set may comprise several million points for the Lorenz attractor — instances where the attractor is represented by a single, elementary cycle (e.g., a figure-eight with one loop on each wing of the Lorenz "butterfly") are readily obtained. This behavior not only epitomizes the essence of the underlying chaotic dynamics but also lends itself to practical application in chaos control problems.

Whereas the above-mentioned publications focused on the discrete images of strange attractors, we propose a method for visualizing the structural nuances of their basins of attraction, employing an analogous discretization philosophy. The spatial patterns manifesting in the resultant visualizations are not state functions; rather, they encode information about processes unfolding in future time intervals within the attractor's basin. This temporal aspect motivates the nomenclature "inverse discrete-dissipative projections." The method's applicability extends beyond chaotic regimes to any scenario involving the compressive deformation of phase volumes. All ensuing results were derived using the Lorenz system [5], a convenient test case owing to its thorough characterization and properties favorable for computation.

The method of inverse discrete-dissipative projections can be regarded as a development of grid/cell-based methods (see, for example, [6-8]). However, all such methods are intended for detecting attractors and their basins, especially in multi-attractor systems. By contrast, the internal structure of basins is usually considered for "continuous" cases, where discretization is performed primarily on the set of initial conditions.

Restricting ourselves to dynamical systems with a single strange attractor, let us outline the main approaches to visualizing the basins of attractors.

Transient structure and convergence time. *Transient-time maps.* Each point of the basin is colored according to the time required for the trajectory to reach a prescribed neighborhood of the attractor; this method reveals slow" regions, attraction channels, long transients, and hidden obstacles inside a single basin [9]. *Finite-time basin stability.* The basin of a single attractor is described by the probability of return within a finite time; the method produces a field or statistics of "fast" and "slow" recovery after perturbation [10]. *Constrained basin stability.* Within the basin, additional constraints on transient trajectories are checked, for example, whether the trajectory remains within an admissible region or returns within a prescribed time; the method therefore shows not only basin membership but also the quality of the transient process [11].

Safe basins. *Safe basin and erosion profiles.* Within the basin, a subset of "safe" initial conditions is identified, that is, initial conditions that do not lead to inadmissible transient deviations; changes in the size of the safe basin under parameter variation are visualized as an erosion profile [12]. *Dynamical integrity measures.* This group of methods measures not only the area or volume of the basin, but also the practical "integrity" of its internal safe part by means of specialized measures [13].

Lyapunov and Zubov fields. *Level sets of a Lyapunov function*. The basin is visualized as a family of nested sublevel sets of a Lyapunov function [14, 15]. *The Zubov function as a coordinate inside the basin*. The Zubov function is used to visualize the internal structure of the basin. Neural-network training of the function for approximating the maximal domain of attraction was proposed in [16]. *Finite-Time Lyapunov Exponent (FTLE) maps:* each point of the basin is colored according to the finite-time Lyapunov exponent, revealing local zones of stretching, compression, and sensitivity to initial conditions [17]. *Fast Lyapunov Indicators (FLI):* initial conditions are colored according to the growth rate of a deviation vector, which makes it possible to reveal regular islands, resonance structures, and chaotic layers inside a single region of motion [18].

Lagrangian descriptors. Each initial point is assigned an integral along the trajectory of a selected geometric or physical quantity over a finite time interval [19-21].

Modern approaches also include the 3D printing of basins of attraction for an illustrative representation of their topology [7].

The subsequent Section 2 delineates the discretization methodology. The visualization technique is defined in Section 3. Section 4 presents the outcomes of its application. A discussion of these results is reserved for Section 5, followed by a concise conclusion and references.

2. Discretization

The discretization method employed in this work constitutes a modification of the approach set forth in [22], affording the derivation of discrete analogues for continuous solutions of systems of ordinary differential equations (ODEs). A discrete trajectory is defined as a sequence of nodes within an a priori defined lattice, generated by an algorithm that prescribes an unambiguous transition rule from a given trajectory point to its successor. Consequently, the discretization procedure reduces to the imposition of a lattice structure and the definition of the aforementioned algorithm, which effects an unambiguous mapping of the lattice onto itself. The requirement of an unambiguous mapping is essential, as it is this property that allows discrete systems to inherit the quintessential characteristic of their continuous counterparts — determinism. However, discrete systems forfeit another critical attribute of their prototypes, guaranteed for ODEs by the Cauchy existence and uniqueness theorem: namely, that through any point in phase space, only a single trajectory may pass. Under the compression of continuous phase volume, discrete trajectories will generally coalesce. This behavior, nevertheless, aptly mirrors the temporal irreversibility inherent to the dissipative systems under consideration.

To enhance computational convenience and efficacy, it is convenient to switch from the time variable t, conventionally the independent variable in ODE systems,

$$\frac{d\vec{x}}{dt} = \vec{v}(\vec{x}, t)$$

to the path-length variable l:

$$\frac{d\vec{x}}{dl} = \frac{\vec{v}(\vec{x}, t)}{\|\vec{v}(\vec{x}, t)\|}, \tag{1}$$

where $\vec{x}$ denotes the state vector and $\vec{v}(\vec{x}, t)$ is the phase velocity. For the Lorenz system, this substitution yields:

$$\begin{cases} \dfrac{dx}{dl} = \dfrac{\sigma(y - x)}{|v|}, \\ \dfrac{dy}{dl} = \dfrac{(r - z)x - y}{|v|}, \\ \dfrac{dz}{dl} = \dfrac{xy - bz}{|v|}, \end{cases} \tag{2}$$

where $|v| = \sqrt{\left(\sigma(y-x)\right)^2 + \left((r-z)x - y\right)^2 + (xy - bz)^2}$. It is crucial to note that system (2) is not equivalent to the original system, as the vector field is now undefined at singular points coinciding with the fixed points of the Lorenz system:

$$C_0 = (0,0,0), C_{\pm} = \left(\pm\sqrt{b(r-1)}, \pm\sqrt{b(r-1)}, r-1\right). \quad (3)$$

This discrepancy, however, is inconsequential for our purposes, as the lattice is constructed such that its nodes avoid these singularities. The transition to length-parameterization is motivated by computational economy, facilitating motion along the trajectory with a fixed step in length rather than time.

The algorithm for iterating the discrete trajectory, illustrated in Fig. 1, comprises two stages:

1. A segment of a "continuous" solution (white circles, Fig. 1) of length L is computed from the initial conditions given by the last point of the discrete trajectory (black circles, Fig. 1), utilizing a fixed-step numerical method. The length L satisfies:

$$L = ab = rk, \quad (4)$$

where a is the lattice constant, r is the step size of the numerical method, k is a positive integer, and b is a positive real number.

2. The terminal point of the segment is then shifted to the nearest lattice node, which subsequently becomes the next point in the discrete trajectory.

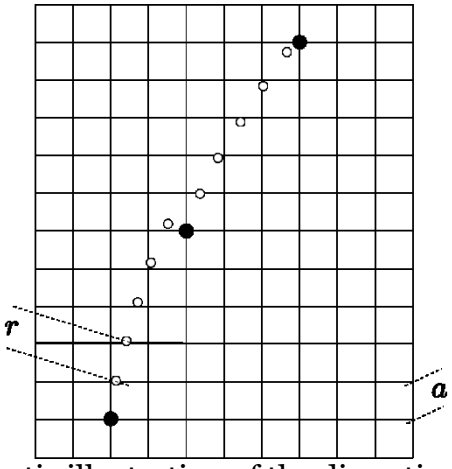


Figure 1. Schematic illustration of the discretization algorithm.

To preclude the intersection of discrete trajectories with the singular point C_0 (3), the lattice is defined to be disjoint from the origin. The procedure for shifting to the nearest lattice node, incorporating this constraint, is given by:

$$\tilde{x}_i = round\left(\frac{x_i}{a}\right)a + \frac{a}{2},$$

where x_i and $\tilde{x}_i$ are the coordinates of the segment endpoint and its nearest lattice node, respectively, and *round(x)* denotes rounding to the nearest integer.

The parameter b in (3), governing the ratio L/a , is conventionally termed the "step on the lattice" and, alongside the lattice constant a, constitutes a pivotal parameter of the algorithm. Although a and b exert a coupled influence on the discretization outcome, their roles can be heuristically decoupled: the lattice constant a primarily governs the resolution of the state vector, whereas the step on the lattice b effectively discretizes the phase velocity vector. Indeed, for a fixed a, the number of attainable subsequent states is dictated by b; larger values of b increase the number of potential transitions, yielding smoother discrete trajectories.

In all experiments reported herein, the 4th-order Runge-Kutta algorithm served as the computational method.

3. Method of Inverse Discrete-Dissipative Projections

The method allows the generation of visualizations for any bounded cross-section of the phase space pertaining to the dynamical system under investigation. The results presented in Section 4 were derived exclusively from two-dimensional cross-sections, which yield 2D images. This restriction was adopted for two principal reasons. First, the present work does not purport to offer a systematic investigation of dynamical systems via the proposed method but is rather devoted to elucidating the method itself. Second, the application of the method entails substantial computational overhead; consequently, generating 3D visualizations, videos, or gathering data from higher-dimensional cross-sections was deemed non-essential within the scope of this introductory work. What follows is a description of the procedure for constructing a 2D image using the method of inverse discrete-dissipative projections.

Consider a 3-dimensional dynamical system. For the sake of definiteness, let us examine a region of the phase space defined by:

$$x \in [x_1, x_2],$$
$$y \in [y_1, y_2],$$
$$z = z_1,$$

where x_1, x_2, y_1, y_2, z_1 are constants. We define the visualization lattice within this specified region as:

$$x_i = x_1 + i\, a\, n_x,$$
$$y_j = y_1 + j\, a\, n_y,$$

where n_x, n_y are positive integer constants, and a is the discretization lattice step. Our experiments employed a square lattice where $n_x = n_y = n$. The set of visualization lattice nodes constitutes a subset of the discretization lattice nodes or coincides with the latter entirely. The number of visualization lattice nodes dictates the resolution of the resultant image.

A cluster comprising the nearest nodes is constructed around each visualization lattice node (see Fig. 2). In our experiments, the cluster was defined as a cube with an edge length of 9 discretization lattice nodes, centered on the visualization lattice node.

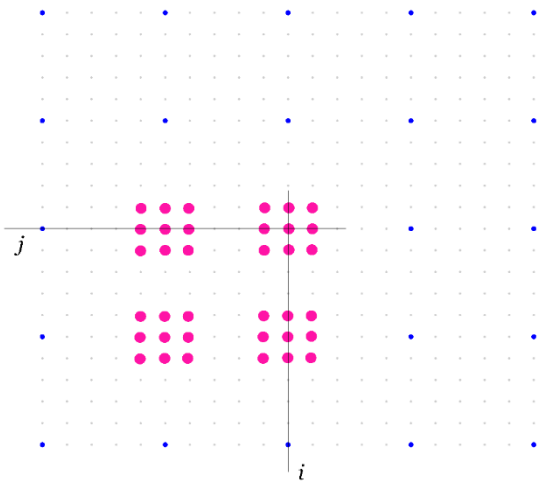


Figure 2. Construction of clusters (red points) around visualization lattice nodes (blue points). Discretization lattice nodes are shown in gray.

Each cluster is treated as a discrete phase volume, where the node count is interpreted as the volume's magnitude. Utilizing the method described in the preceding section, discrete trajectories are computed for the points within these clusters. At each computational step, the volume of the discrete cluster — that is, the count of its unique points — is evaluated. In the general case, discrete trajectories will coalesce, leading to a reduction in the number of unique points within the cluster. This yields a function describing the dependence of the unique point

count (the discrete phase volume) on the number of computational steps. Given that one computational step corresponds to the evolution of the dynamical system's trajectory over a fixed length (up to the lattice step), we obtain, to a certain approximation, a function representing the phase volume's dependence on trajectory length.

For all initial visualization lattice nodes, the number of discrete trajectory computation steps is fixed at a value N, chosen such that all trajectories are guaranteed sufficient time to reach the discrete attractor, i.e., one of the cycles. For each functional dependence, the following quantity is computed:

$$\mu(i,j) = \sum_{k=1}^{N} m_k(i,j), \tag{5}$$

where $m_k(i,j)$ is the number of unique points in the cluster defined at the visualization lattice node with coordinates (i,j) (see Fig. 2) after k steps of the discretization method. Finally, we assign to each visualization lattice node with coordinates (i,j) within the selected region its corresponding value $\mu(i\,,j)$. Mapping the $\mu(i\,,j)$ values to colors according to a specified color palette (see the next section) yields the final image. Thus, each point in the image generated by the method of inverse discrete-dissipative projections encodes information about the evolutionary character of a bundle of trajectories emanating from the vicinity of the corresponding point in the dynamical system's phase space.

The constant N in (5) is determined empirically, and its value can be established via one of two approaches. Both require the computation of a discrete trajectory for each visualization lattice node. The first approach halts computations upon the trajectory's entry into a cycle; the second, upon its closure. This approach requires prior knowledge of the complete set of cycles (cf. [2]). Although simpler to implement, the second approach may require considerable redundant computation, performed after the trajectory has entered a cycle but before it formally closes. We employed the first approach.

It is noteworthy that the dependencies of the discrete volumes on the number of computational steps are quite informative in their own right and could be utilized to construct more sophisticated and detailed characteristics beyond the scalar quantities defined in (5).

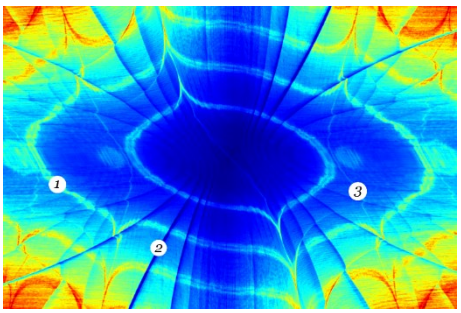
4. Results

The results presented in this section were obtained for the modified Lorenz system (2). The color palette used for visualization is shown in Fig. 3. This palette comprises 256 colors. The minimum and maximum values of $\mu(i\,,j)$ are mapped to the leftmost (dark blue) and rightmost (dark red) colors of the palette, respectively.

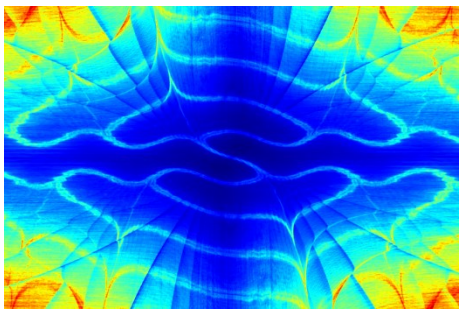


Figure 3. Color palette used for visualization.

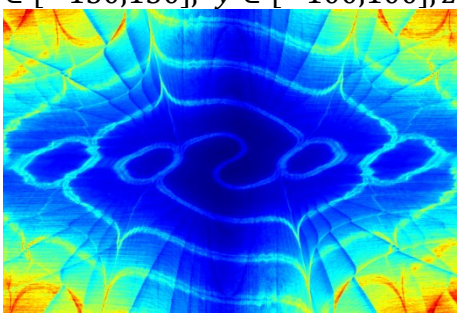
The first set of images (Figs. 4 and 5) corresponds to the case of non-chaotic dynamics with system parameters: $b = \frac{8}{3}, \sigma = 10, r = 18$. Discretization parameters were: $a = 0.0764, b = 10$. The visualization lattice step was 0.1528. Images (4.A,B,C) represent regions in planes parallel to the XY coordinate plane at $z = 0, 19,$ and 28. The region dimensions are $x \in [-150,150]$, $y \in [-100,100]$. Fig. 4.D shows the visualization for the region $x = 0, y \in [-150,150], z \in [-80,120]$. Fig. 5 presents a 3D composite image constructed from regions lying in the coordinate planes $X = 0, Y = 0$ and the plane $Z = 28$. The respective dimensions are indicated on the figure.



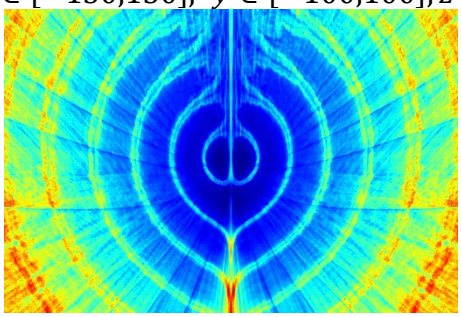
$A.\ x \in [-150,150],\ y \in [-100,100], z = 0.$



$B.\ x \in [-150,150],\ y \in [-100,100], z = 19.$



$C.\ x \in [-150,150],\ y \in [-100,100], z = 28.$



$D.\ x = 0, y \in [-150,150],\ z \in [-80,120].$

Figure 4. Visualization results: A, B, C – cross-sections parallel to the XY plane, D – cross-section in the YZ plane.

A complex spatial structure is distinctly visible. At least three types of configurations can be identified (see annotations on Fig. 4.A). The first and most prominent structure 1 partitions the discrete phase space into numerous cells of non-trivial topology. Furthermore, the boundaries between these cells are characterized by significantly higher values of the criterion (5) compared to the cells' interior regions. It will be demonstrated in the subsequent set of images that this structure loses its sharp boundaries upon the transition to chaotic dynamics. However, this structure appears to be invariant under refinement of the discretization lattice. Structure 2, referred to below as "folds," is instead a direct consequence of the applied discretization algorithm. It will be illustrated below that increasing the discretization parameter b (step on the lattice) leads to an increase in the number of these folds. We expect that for large b the folds should become visually indistinguishable. Finally, there is structure 3, discernible as a fine network that occasionally intersects with structure 1. This structure, while undergoing some modifications, persists upon the transition to deterministic chaos.

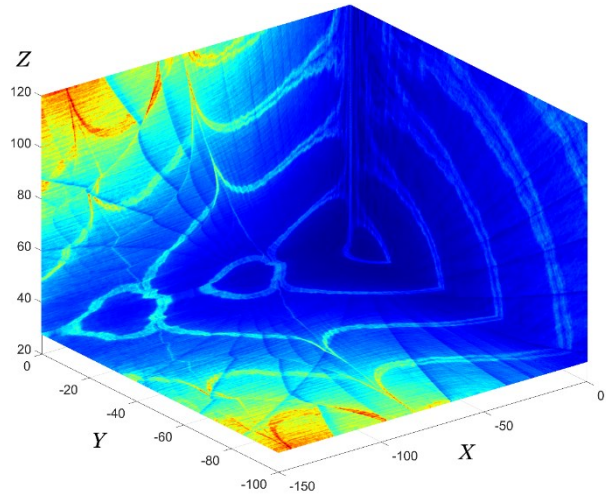


Figure 5. 3D visualization composite for regions lying in the coordinate planes $X = 0, Y = 0$ and the plane $Z = 28$.

Let us now consider the case of chaotic dynamics under the “classical” parameters of the Lorenz system: $b = \frac{8}{3}, \sigma = 10, r = 28$. Figs. 6 and 7 provide illustrations analogous to Fig. 4C, i.e., for the visualization region $x \in [-150,150],\ y \in [-100,100], z = 28$. Figs. 6 and 7 differ in their discretization parameters. For Fig. 6: $a = 0.06, b = 10$. For Fig. 7: $a = 0.03, b = 20$. The visualization lattice step is 0.12 in both cases. Increasing b increases the density of folds. A visualization with discretization parameters $a = 0.03, b = 10$ is virtually identical to that in Fig. 6 and is therefore not shown. This confirms that the fold density is determined specifically by the parameter b.

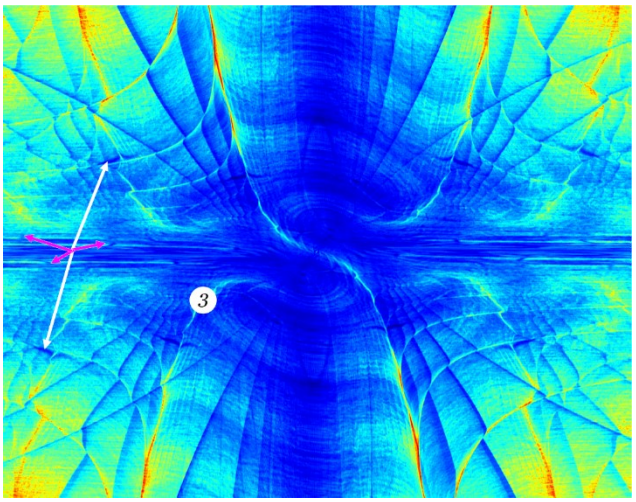


Figure 6. Chaotic dynamics. Visualization region: $x \in [-150,150],\ y \in [-100,100], z = 28$. Discretization parameters: $a = 0.06, b = 10$.

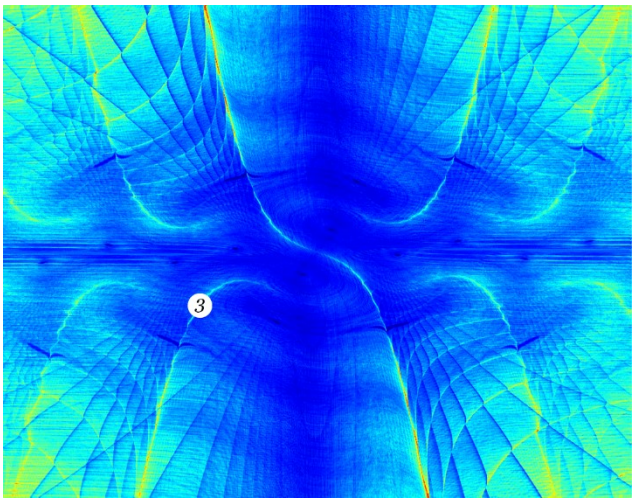


Figure 7. Chaotic dynamics. Visualization region: $x \in [-150,150],\ y \in [-100,100], z = 28$. Discretization parameters: $a = 0.03, b = 20$.

Visual analysis of Figs. 6 and 7, along with other similar images for the chaotic regime, indicates that structure 1 (Fig. 4A) disintegrate significantly, leaving behind traces in the form of blurred boundaries. However, structure 3 (Fig. 4A) persist (see circular markers with the number 3). On the basis of our preliminary results, we hypothesize that this structure possesses an invariant component with respect to the discretization parameters and thus likely has a counterpart in the original continuous system.

In addition to the structures considered, areas with anomalously rapid reduction of discrete phase volumes are visible in Figs. 6 and 7 (indicated by white and pink arrows in Fig. 6). They are more clearly defined in Fig. 7. It can be demonstrated that these areas correspond to two spirals terminating in the vicinity of the attractor's fixed points. Located near these fixed points

are trivial cycles – rings. Thus, it can be asserted that the majority of discrete trajectories constituting the spirals terminate precisely on these rings. Some rings may be degenerate, consisting of a single point. The total number of rings can reach several dozen, but in terms of point count, the rings generally contribute insignificantly compared to the remaining cycles.

All demonstrated images were generated using original software written in C++ utilizing the CUDA framework. The creation of visualization images requires substantial computational resources, justifying the use of many-core graphics processing units (GPUs).

5. Discussion

Analysis of the results obtained through the application of the inverse discrete-dissipative projections method yields insights into the behavioral patterns of discretized dynamical systems in the vicinity of their attractors. As noted in the introduction, we invariably deal with such systems when simulating them algorithmically; thus, the scientific value of this line of inquiry is evident. Within this context, a set of questions arises, the thorough investigation of which extends beyond the scope of the present work. However, one particular set of issues warrants immediate discussion: namely, what is the nature of the mechanism responsible for the emergence of structure 1 and 3 (Fig. 4), and do they bear any relation to the original mathematical models?

A defining characteristic of structure 1 and 3 is the relatively high value of criterion (5) at their boundaries compared to the values observed within the regions. Based on the conducted numerical experiments, a plausible hypothesis can be advanced: in most cases, structures 1 and 3 coincide with the boundaries separating regions from which trajectories reach the attractor at different times. A discrete phase volume initiating its evolution precisely on the boundary between two such regions will, with high probability, split into two subsets, one of which reaches the attractor sooner than the other. Consequently, the reduction rate of such a volume will be lower compared to volumes evolving from within the cells defined by the boundaries of structures 1 and 3. Thus, the visualization method effectively highlights the boundaries between regions characterized by “divergent” system behavior. An analogy can be drawn here with the application of filters in convolutional neural networks, which are used to detect edges separating areas of differing intensity, color, etc., in images.

Regarding the potential modification or further development of the method, emphasis should be placed on refining criterion (5). It is conceivable that defining a more complex characteristic — for instance, employing various types of filters constructed upon the functional dependency underlying criterion (5) — could yield more profound information about the behavior of the dynamical system under investigation.

6. Conclusion

A method for visualizing the structural features of attractor basins in discretized dynamical systems has been proposed. Numerical experiments were conducted, and their results were presented, forming the basis for conclusions regarding both the structures revealed through visualization and the operational specifics of the method itself. The method was tested on the Lorenz system, considering two types of attractors: a limit cycle and a strange attractor. The visualizations reveal complex spatial organizations, including persistent fine-scale networks and discretization-induced folds, whose properties and origins were analyzed. The method provides a tool for investigating the interplay between the inherent properties of continuous dynamical systems and the artifacts introduced by their necessary discretization for computational study, opening avenues for further research into the geometric structure of basins of attraction in algorithmic simulations.

References

1. Kunin I., Chernykh G., Kunin B. Optimal chaos control and discretization algorithms // International Journal of Engineering Science, Vol. 44, № 1–2, 2006, pp. 59–66 (doi:10.1016/j.ijengsci.2005.05.006)
2. Chernykh, G. Stable and chaotic modes in discrete dynamic systems (Lorenz attractor and Kropotov-Pakhomov neural network model). PhD thesis in physics and mathematics. St. Petersburg, 2004, 103 p.
3. Yamrom B., Kunin I., Chernykh G. Centroidal trajectories and frames for chaotic dynamical systems // International Journal of Engineering Science, Vol. 41, 2003, pp. 465–473 (doi: 10.1016/S0020-7225(02)00217-3)
4. Li M., Vitányi P. An Introduction to Kolmogorov Complexity and Its Applications. Cham: Springer, 2019. 834 p. (doi:10.1007/978-3-030-11298-1)
5. Lorenz E. N. Deterministic nonperiodic flow // Journal of the Atmospheric Sciences, Vol. 20, 1963, pp. 130–141 (doi:10.1175/1520-0469(1963)020%3C0130:DNF%3E2.0. CO;2) (https:// journals.ametsoc.org/downloadpdf/view/journals/atsc/20/2/1520-0469 _1963_020_0130_dnf_2_0_co_2.pdf)
6. Datseris G., Wagemakers A. Effortless estimation of basins of attraction // Chaos, Vol. 32, № 2, 2022, 023104 (doi:10.1063/5.0076568)
7. Xiong A., Sprott J. C., Lyu J., Wang X. 3D Printing — The Basins of Tristability in the Lorenz System // International Journal of Bifurcation and Chaos, Vol. 27, № 8, 2017, 1750128 (doi:10.1142/S0218127417501280) (https://sprott.physics.wisc.edu/pubs/paper 477.htm)
8. Daza A., Wagemakers A., Sanjuán M. A., Yorke J. A. Testing for Basins of Wada // Scientific Reports, Vol. 5, 2015, 16579 (doi:10.1038/srep16579)
9. Ray A., Pal A., Ghosh D., Dana S. K., Hens C. Mitigating long transient time in deterministic systems by resetting // Chaos, Vol. 31, № 1, 2021, 011103 (doi:10.1063/ 5.0038374)
10. Schultz P., Hellmann F., Webster K. N., Kurths J. Bounding the first exit from the basin: Independence times and finite-time basin stability // Chaos, Vol. 28, № 4, 2018, 043102 (doi:10.1063/1.5013127)
11. van Kan A., Jegminat J., Donges J. F., Kurths J. Constrained basin stability for studying transient phenomena in dynamical systems // Physical Review E, Vol. 93, № 4, 2016, 042205 (doi:10.1103/PhysRevE.93.042205)
12. Soliman M. S., Thompson J. M. T. Integrity measures quantifying the erosion of smooth and fractal basins of attraction // Journal of Sound and Vibration, Vol. 135, № 3, 1989, pp. 453-475 (doi:10.1016/0022-460X(89)90699-8)
13. Rega G., Lenci S. Dynamical Integrity and Control of Nonlinear Mechanical Oscillators // Journal of Vibration and Control, Vol. 14, № 1-2, 2008 (doi:10.1177/1077546307079403)
14. Zhai C., Nguyen H. D. Estimating the Region of Attraction for Power Systems Using Gaussian Process and Converse Lyapunov Function // IEEE Transactions on Control Systems Technology, Vol. 30, № 3, 2022, pp. 1328-1335 (doi:10.1109/TCST.2021. 3098167)
15. Mohammadi H., Peet M. M. Estimating the Region of Attraction Using Polynomial Optimization: a Converse Lyapunov Result // arXiv preprint arXiv:1704.06983, 2017 (https://arxiv.org/abs/1704.06983)
16. Liu J., Meng Y., Fitzsimmons M., Zhou R. Towards Learning and Verifying Maximal Neural Lyapunov Functions // 2023 62nd IEEE Conference on Decision and Control (CDC), Singapore, Singapore, 2023, pp. 8012-8019 (doi:10.1109/CDC49753.2023. 10383299)
17. Shadden S. C., Lekien F., Marsden J. E. Definition and properties of Lagrangian coherent structures from finite-time Lyapunov exponents in two-dimensional aperiodic flows // Physica D: Nonlinear Phenomena, Vol. 212, № 3-4, 2005, pp. 271-304 (doi:10.1016/j.physd.2005. 10.007)
18. Darriba L. A., Maffione N. P., Cincotta P. M., Giordano C. M. Comparative study of variational chaos indicators and ODEs' numerical integrators // International Journal of Bifurcation and Chaos, Vol. 22, № 10, 2012, 1230033 (doi:10.1142/S0218127412300339)

19. García-Garrido V. J., García-Luengo J. Painting the phase space of dissipative systems with Lagrangian descriptors // Communications in Nonlinear Science and Numerical Simulation, Vol. 104, 2022, 106034 (doi:10.1016/j.cnsns.2021.106034)

20. Agaoglou M., García-Garrido V. J., Katsanikas M., Wiggins S. Visualizing the phase space of the HeI2 van der Waals complex using Lagrangian descriptors // Communications in Nonlinear Science and Numerical Simulation, Vol. 103, 2021, 105993 (doi:10.1016/j.cnsns. 2021.105993)

21. Daquin J., Pédenon-Orlanducci R., Agaoglou M., García-Sánchez G., Mancho A. M. Global dynamics visualisation from Lagrangian Descriptors. Applications to discrete and continuous systems // Physica D: Nonlinear Phenomena, Vol. 442, 2022, 133520 (doi:10.1016/j.physd. 2022.133520)

22. Rannou F. Numerical study of discrete plane area-preserving mappings // Astronomy and Astrophysics, Vol. 31, 1974, pp. 289–301 (https://ui.adsabs.harvard.edu/abs/ 1974A%26A.... 31..289R)